

# Kinetic arrest in polyion-induced inhomogeneously charged colloidal particle aggregation

D. Truzzolillo, F. Bordi, F. Sciortino, and C. Cametti<sup>a</sup>

Dipartimento di Fisica, Università di Roma “La Sapienza” Piazzale A. Moro 5, I-00185 - Roma, Italy  
and INFM CRS-SOFT, Unità di Roma 1, Roma, Italy

Received 18 December 2008

Published online: 24 June 2009 – © EDP Sciences / Società Italiana di Fisica / Springer-Verlag 2009

**Abstract.** Polymer chains adsorbed onto oppositely charged colloidal particles can significantly modify the particle-particle interactions. For sufficient amounts of added polymers, the original electrostatic repulsion can even turn into an effective attraction and relatively large aggregates can form. The attractive interaction contribution between two particles arises from the *correlated* adsorption of polyions at the oppositely charged particle surfaces, resulting in a non-homogeneous surface charge distribution. Here, we investigate the aggregation kinetics of polyion-induced colloidal complexes through Monte Carlo simulation, in which the effect of charge anisotropy is taken into account by a DLVO-like inter-particle potential, as recently proposed by Velegol and Thwar (Langmuir **17**, 7687 (2001)). The results reveal that the aggregation process slows down due to the progressive increase of the potential barrier height upon clustering. Within this framework, the experimentally observed cluster phases in polyelectrolyte-liposome solutions can be interpreted as a kinetic arrested state.

**PACS.** 64.70.pv Colloids – 82.70.Dd Colloids – 89.75.Fb Structures and organization in complex systems

## 1 Introduction

The addition of oppositely charged polyions to a suspension of charged colloidal particles gives rise to an intriguing and partially unexpected phenomenology [1–4], resulting in the formation of particle aggregates which play an important role in a wide range of implications [5–7], from membrane biophysics and soft matter physics [8–10] to biotechnological processes, such as therapeutic delivery systems [11].

These aggregates are governed by a delicate balance between attractive and repulsive interactions resulting in the appearance of stable, kinetically arrested cluster phase, where single particles stuck and form relatively large complexes. In this system, the short-range attraction contribution is promoted by the addition of “adsorbing” polyions which form a two-dimensional strongly correlated, short-range-ordered, structure on the surface of the oppositely charged particle, contrarily to what happens for “non-adsorbing” polymers, where the attraction contribution is produced by the unbalanced osmotic pressure in the depletion regime.

Correlated adsorption of polyion chains on the surface of oppositely charged particles (“charge patch” attraction) induces two different phenomena: “charge inversion” [1, 2, 8, 9] and “re-entrant condensation” [1, 2, 12].

The first one occurs when a colloidal particle binds several oppositely charged multi-valent ions (polyions), so that its net effective charge inverts its sign. The second effect, concomitant to the charge inversion, consists in the formation of particle aggregates whose average size increases on increasing the polyion concentration, until it reaches a maximum (at the point of charge inversion), decreasing afterwards to the initial value.

The formation of these polyion-induced charged-particle aggregation is largely independent of the choice of the particular system we are dealing with, and the same basic phenomenology has been observed in the case of “*soft*” particles, such as for example DOTAP liposomes interacting with anionic polyions [1] and hybrid niosomes interacting with cationic polymers [13], and, also, in the case of “*solid*” particles, such as positively charged lipid-covered polystyrene particles interacting with synthetic or natural anionic polymers [14], or negatively charged polystyrene spheres interacting with cationic polyelectrolytes [15].

The occurrence of a sharp re-entrant condensation on increasing the adsorption of polyion on charged liposomes, accompanied by a giant charge inversion, has been documented for high dilute concentration regime in a series of papers [1, 2, 12], although it is well known that for higher concentrations structural rearrangements are in principle possible and in particular condition of concentration, observed [16, 17].

<sup>a</sup> e-mail: cesare.cametti@roma1.infn.it

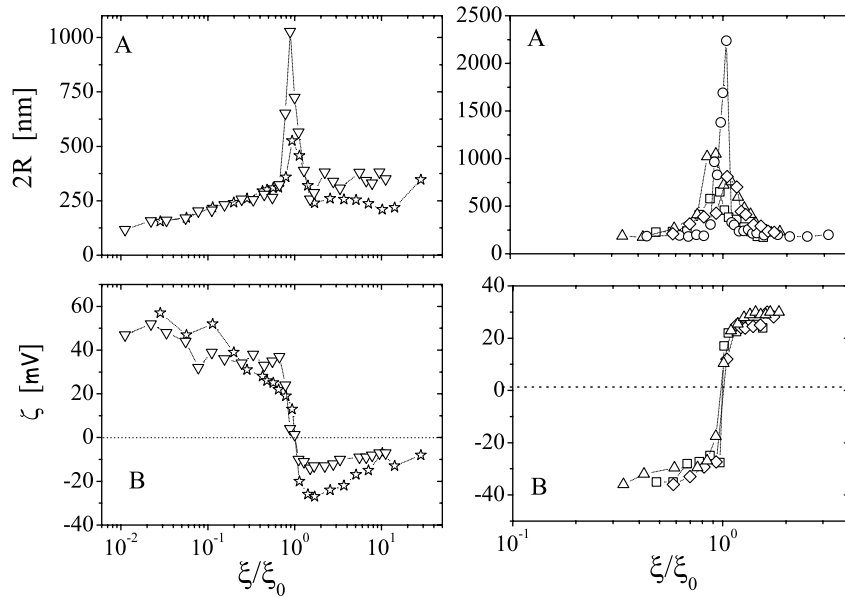


**Fig. 1.** A brief review of the experimental evidence of re-entrant condensation and charge inversion in polyion-induced charged-particle aggregates, in the presence of oppositely charged polyions in the case of *soft* particles (liposomes and hybrid niosomes). Left panels: re-entrant condensation (aggregate radius  $R$ ) (A) and charge inversion ( $\zeta$ -potential) (B) of positively charged liposomes, in the presence of negatively charged polyions. Right panels: re-entrant condensation (aggregate size  $R$ ) (A) and charge inversion ( $\zeta$ -potential) (B) of negatively charged hybrid niosomes, in the presence of positively charged polyions. The data are shown as a function of the charge molar ratio  $\xi$  normalized to the value  $\xi_0$  at which the measured  $\zeta$ -potential goes to zero.  $\xi$  is defined as the polyion to the lipid molar ratio. The experimental values (hydrodynamic radius measured by means of dynamic light scattering and  $\zeta$ -potential measured by means of Doppler laser electrophoretic techniques) refer to different colloidal systems. Positive charged particles:  $\nabla$ : DOTAP liposomes (0.8 mg/ml) and polyacrylate sodium salt;  $\star$ : DOTAP liposomes (1.7 mg/ml) and polyacrylate sodium salt [12]. Negative charged particles:  $\circ$ : hybrid niosomes and  $\alpha$ -polylysine;  $\triangle$ : hybrid niosomes and  $\epsilon$ -polylysine;  $\diamond$ : hybrid niosomes and PEVP (ionization degree 95%) [13]. Hybrid niosomes are built up by Tween20, cholesterol and dicetylphosphate and the cationic polyion PEVP is Poly[*N*-ethyl-4-vinyl pyridinium] bromide.

It has been shown that, both for *soft* and *solid* particles, the size of the aggregates goes through a maximum and their overall charge inverts its sign in concomitance to the point of charge inversion, as briefly reviewed in fig. 1 and fig. 2 for some typical cationic or anionic colloidal particle (*soft* particles) systems and for some typical *solid* particle systems, respectively. These examples are strongly suggesting the existence of a cluster phase consisting of intact charged particles stuck together by electrostatic interactions due to the adsorption of oppositely charged polyions (see [18]).

The formation of aggregates and, consequently, the stability of colloidal charged particles (*solid* particles or *soft* vesicles) is usually satisfactorily explained in the framework of Derjaguin-Landau-Verwey-Overbeek (DLVO) theory [19], which accounts for electrostatic and van der Waals interactions between two approaching particles. In the traditional DLVO theory, the particle surface is assumed to be uniformly charged.

In the case of polyion-correlated adsorption onto the surface of the particle, this assumption is no longer valid and the classic DLVO theory might not account for the effects arising from the surface charge heterogeneity. Indeed, the adsorption of the polymer generates an ordered charged structure (“patchy charge distribution”), strongly dependent on the polyion size, on the valence and on the

linear charge density [8]. Some experimental evidences of such a structure can be found in refs. [12,13,20]. In this respect, it is reasonable to expect that attractive interactions can arise when “counterion domains” on one particle align to “counterion-free domains” on another approaching particle, giving rise to the short-range attractive contribution.

Recently, Velegol and Thwar [21] have developed an analytical model for the effective particle-particle potential  $\langle \Phi \rangle$  in the case of non-uniform charge distributions, based on the Derjaguin approximation and on an extension of the Hogg-Healy-Fuerstenau (HHF) [22] model for randomly charged surfaces. The resulting spherically symmetric potential depends on the values of the average surface potential (here assumed equal to the  $\zeta$ -potential) and on the standard deviation  $\sigma$  of the surface potential among different regions on the particle surface.

In this manuscript, we analyze the aggregation process of spherical charged particles interacting via the Velegol and Thwar [21] potential by means of MC simulation. Starting from isolated monomers, we follow the growth of the aggregates until a kinetically arrested state is reached. We study the final size of the aggregates for several values of the  $\zeta$ -potential and its standard deviation  $\sigma$ . The results of the simulations confirm that the final size of the aggregates grows on increasing the standard deviation  $\sigma$

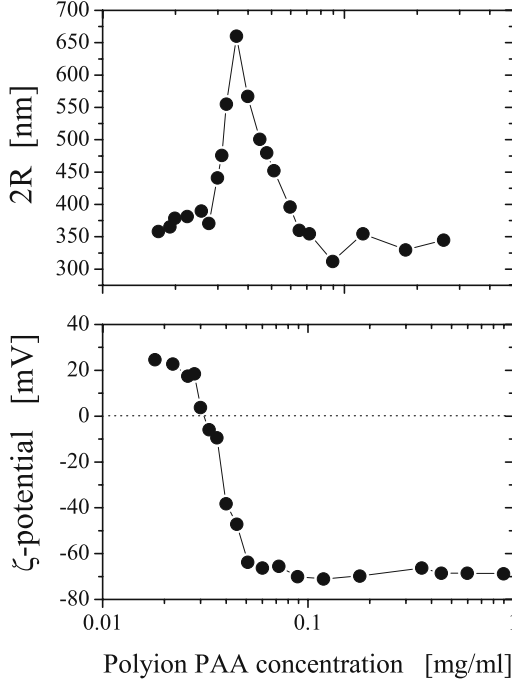


**Fig. 2.** Re-entrant condensation and charge inversion in polyion-induced charged-particle aggregates in the case of “solid” particles (polystyrene spheres). Upper panel: the diameter  $2R$  of aggregates of lipoparticles (polystyrene particles covered by a DOTAP lipid layer) as a function of the oppositely charged polyion concentration (the behavior is typical of the re-entrant condensation effect). Bottom panel: the  $\zeta$ -potential of the aggregates as a function of the polyion concentration. The charge inversion effect changes the overall charge of the aggregates from positive (lipoparticles in the absence of polyions) to negative after the adsorption in excess of polyion chains.

and on decreasing the  $\zeta$ -potential, providing a microscopic interpretation of the re-entrant condensation and charge inversion phenomena in polyion-induced charged colloidal particle aggregation.

## 2 Theoretical background

According to the HHF model [22], the electrostatic potential of mean force  $\Phi$  between two dielectric colloidal spherical particles of radius  $R_A$  and  $R_B$  and surface potentials  $\psi_A$  and  $\psi_B$ , respectively, is given by

$$\Phi_{AB} = \frac{\epsilon\pi R_A R_B}{R_A + R_B} \left[ (\psi_A^2 + \psi_B^2) \ln(1 - e^{-2\kappa H}) + 2\psi_A \psi_B \ln \left( \coth \frac{\kappa H}{2} \right) \right]. \quad (1)$$

Here,  $\epsilon$  is the dielectric permittivity of dispersing medium,  $\kappa^{-1}$  is the Debye screening length and  $H$  is the minimal distance between the two particle surfaces (see fig. 3). Equation (1), which is derived under the conditions  $\kappa R_\alpha \gg 1$  and  $H/R_\alpha \ll 1$  ( $\alpha = A, B$ ), holds under the following assumption: i)  $\psi_A$  and  $\psi_B$  are relatively small

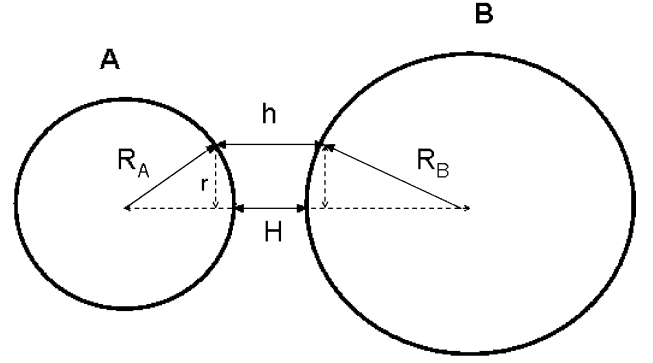


**Fig. 3.** Variables involved in the Derjaguin approximation, for two approaching particles of radius  $R_A$  and  $R_B$ , respectively.

(less than 25 mV at room temperature); ii) the particles share the same chemical nature and are charged by similar mechanism; iii) the Derjaguin approximation holds [19].

Velegol and Thwar [21] assume that the surface of a particle of type  $\alpha$  is partitioned in  $N$  regions (labelled by  $i$ , with  $i = 1, \dots, N_\alpha$ ) of area  $S$ , each of them characterized by a different value of the surface potential  $\psi_\alpha^i$ . These regions must be of sufficient size  $L \sim \sqrt{S}$ , so that lateral interactions can be considered negligible (practically this means that  $L \gg \kappa^{-1}$  and  $L \ll H$ ). The surface potentials  $\psi_A$  and  $\psi_B$  of two approaching particles in the HHF theory are thus replaced with the random value of the potential  $\psi_A^i$  and  $\psi_B^j$ , where  $i$  and  $j$  label the two domains (on opposite particles) facing each other. Defining  $\zeta_\alpha$  as the average potential, one can write  $\psi_\alpha^i \equiv \zeta_\alpha + \delta_\alpha^i$  where  $\delta_\alpha^i$  a random contribution that varies among the different regions. The  $\delta_\alpha^i$  are independently distributed and not correlated, *i.e.*

$$\langle \psi_\alpha^i \psi_\beta^j \rangle = \begin{cases} \zeta_\alpha^2 + \sigma_\alpha^2 \delta^{ij}, & \text{if } \alpha = \beta = A, \\ \zeta_A \zeta_B, & \text{if } A \neq B, \\ \zeta_B^2 + \sigma_B^2 \delta^{ij}, & \text{if } \alpha = \beta = B, \end{cases} \quad (2)$$

where  $\delta^{ij}$  is the Kröenecker delta function and  $\sigma_\alpha$  the standard deviation of surface potential on spheres of type  $\alpha$ .

The expression for the resulting potential of mean force provided by Velegol and Thwar [21] is

$$\Phi_{AB} = \frac{\epsilon\kappa}{2} \sum_{i=1}^M \left\{ (\zeta_A^2 + \zeta_B^2 + 2\zeta_A \delta_i^A + 2\zeta_B \delta_i^B + \delta_A^2 + \delta_B^2)(1 - \coth \kappa h_i) + \frac{2(\zeta_A + \delta_i^A)(\zeta_B + \delta_i^B)}{\cosh \kappa h_i} \right\} S, \quad (3)$$

where the sum runs over the  $M$  facing regions and  $h_i$  is the gap between  $i$ -th regions. The ensemble averaging gives

$$\langle \Phi_{AB} \rangle = \frac{\epsilon\kappa}{2} \sum_{i=1}^M \left\{ (\zeta_A^2 + \zeta_B^2 + \sigma_A^2 + \sigma_B^2)(1 - \coth \kappa h_i) + \frac{2\zeta_A \zeta_B}{\cosh \kappa h_i} \right\} S. \quad (4)$$

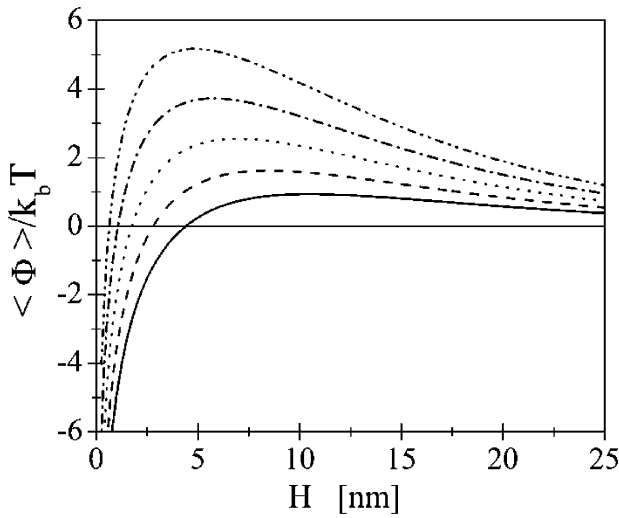


**Fig. 4.** Mean-force potential profiles ( $\langle \Phi_{AA} \rangle$ ) between two identical spheres ( $A = B$ ) calculated from eq. (7) for different values of  $\zeta_A = \zeta_B = \zeta$  (from 11 to 19 mV) and for a constant value of  $\sigma_A = \sigma_B = \sigma = 15$  mV. Curves are plotted in units of the thermal energy  $k_b T$  at room temperature for  $R_A = R_B = R = 40$  nm and  $\kappa^{-1} = 10$  nm. Solid line:  $\zeta = 11$  mV; dashed line:  $\zeta = 13$  mV; dotted line:  $\zeta = 15$  mV; dot-dashed line:  $\zeta = 17$  mV; double-dot dashed line:  $\zeta = 19$  mV.

In order to evaluate the sum in eq. (4), the Derjaguin approximation is applied (fig. 3), *i.e.*

$$h \approx H + \frac{R_A + R_B}{2R_A R_B} r^2 \quad (5)$$

and, for any function  $F(h)$ , the following expressions are employed:

$$\sum_{i=1}^M F(h_i) A_i \approx 2\pi \frac{R_A R_B}{R_A + R_B} \int_0^{+\infty} F(h) dh, \quad (6)$$

where  $r$  is the flat ring radius (see fig. 3).

The resulting mean force pair interaction potential is given by

$$\langle \Phi_{AB} \rangle = \frac{\epsilon\pi R_A R_B}{R_A + R_B} \left[ (\zeta_A^2 + \zeta_B^2 + \sigma_A^2 + \sigma_B^2) \ln(1 - e^{-2\kappa H}) + 2\zeta_A \zeta_B \ln \left( \coth \frac{\kappa H}{2} \right) \right]. \quad (7)$$

The mean force potential for typical values of the  $\zeta$ -potential and standard deviation  $\sigma$  is shown in figs. 4 and 5. The potential combines a repulsive net charge-dependent monopole term ( $\zeta_\alpha \neq 0$ ) and an attractive multipole term ( $\sigma_\alpha \neq 0$ ) arising from the presence of random charge heterogeneity on the particle surface, leading up to the presence of a potential barrier. In the case of particles with the same net charge, an attractive component is always present since the first term in eq. (7) is negative. If the two identical particles are uniformly charged

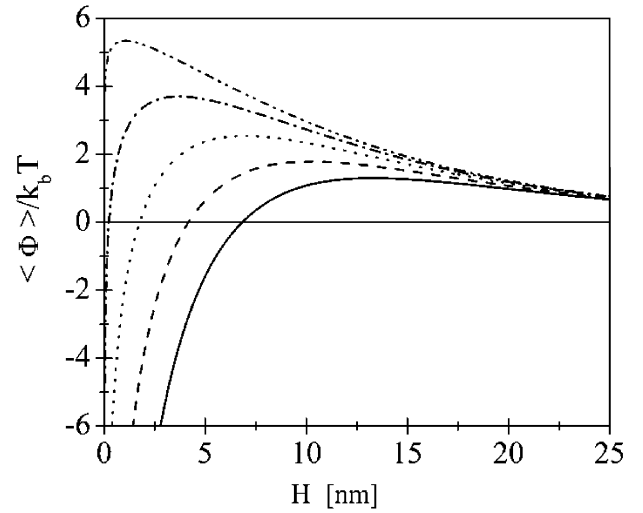


**Fig. 5.** Mean-force potential profiles between two identical spheres calculated from eq. (7) for different values of  $\sigma_A = \sigma_B = \sigma$  (from 5 to 25 mV) and for a constant value of  $\zeta_A = \zeta_B = \zeta = 15$  mV. Curves are plotted in units of the thermal energy  $k_b T$  at room temperature for  $R_A = R_B = R = 40$  nm and  $\kappa^{-1} = 10$  nm. Solid line:  $\sigma = 25$  mV; dashed line:  $\sigma = 20$  mV; dotted line:  $\sigma = 15$  mV; dot-dashed line:  $\sigma = 10$  mV; double-dot dashed line:  $\sigma = 5$  mV.

( $\sigma_\alpha = 0$ ), both the attractive component and the global maximum vanish, recovering the HHF expression for two identical spheres (eq. (1)).

The height of the potential barrier that two approaching particles must overcome in order to aggregate and the distance between the particle surface at which this maximum occurs can be evaluated from eq. (7). For two identical particles ( $R_A = R_B = R$ ) we obtain:

$$\langle \Phi_{AB} \rangle_{\max} = \pi\epsilon R \left\{ (\zeta^2 + \sigma^2) \ln \left[ 1 - \left( \frac{\zeta^2}{\zeta^2 + \sigma^2} \right)^2 \right] + \zeta^2 \ln \left[ \frac{2\zeta^2 + \sigma^2}{\sigma^2} \right] \right\} \quad (8)$$

and

$$H_{\max} = \frac{1}{\kappa} \ln \left( \frac{\zeta^2 + \sigma^2}{\zeta^2} \right). \quad (9)$$

We point out that in the Velegol and Thwar model: i) the height of the potential barrier does not depend on the Debye screening length  $\kappa^{-1}$ . Consequently, addition of simple salt in bulk phase (varying the ionic strength of the solvent) does not change the strength of the interaction but only modifies the distance at which this maximum interaction occurs; ii) using Derjaguin approximation, a linear dependence of the barrier height on the radius  $R$  of the particles arises, underlying that larger particles interact more intensely than smaller ones and thus aggregation in the presence of large clusters is relatively inhibited; iii)  $\langle \Phi \rangle_{\max}$  is zero when  $\zeta = 0$  and  $\lim_{\sigma \rightarrow 0^+} H_{\max} = 0$ , that is consistent with the statement that there is no attractive component for uniformly charged particles and that

a lower value of  $\sigma$  determines a short-ranged attractive interaction.

Colloidal particles with smaller curvature radius, lower  $\zeta$ -potential or higher charge anisotropy will be characterized by a faster aggregation dynamics. The aggregation process will slow down due to the progressive increase of the repulsive barrier on increasing the size of the aggregates.

In the next section, we introduce a MC simulation method to analyze the aggregation dynamics of spherical clusters and to evaluate the evolution of the mean cluster radius for several values of  $\zeta$ -potential and standard deviation  $\sigma$ , chosen to model the corresponding experimental range of values observed for polyion-induced liposome cluster aggregation (fig. 1).

In our calculations, the contribution to the attraction associated to the van der Waals interaction between two approaching particles is neglected. The reason why such interaction can be safely neglected arises from the typical range associated to the van der Waals interaction, which dies off before  $H_{\max}$ . Indeed, for liposome particles (aqueous cores of radii  $R_1$  and  $R_2$ , respectively, covered by phospholipid shell of thickness  $d$ ), the van der Waals interaction  $V_{\text{vdW}}$  can be written as [23]

$$V_{\text{vdW}} = -\frac{AR_1R_2}{6(R_1+R_2)} \left[ \frac{1}{H+2d} - \frac{2}{H+d} + \frac{1}{H} \right] - \frac{A}{6} \ln \left[ \frac{H(H+2d)}{2(H+d)} \right] \quad (10)$$

(where  $A$  is the Hamaker constant). For typical values of the parameters involved, eq. (10) results in a range of attraction which becomes negligible beyond 1–2 nm. As can be seen from figs. 4 and 5, this distance is always smaller than  $H_{\max}$ . Consequently, we neglect the van der Waals interaction in the irreversible aggregation process.

### 3 Simulation

We study a system composed of  $N_p = 10000$  colloidal particles of initial diameter  $2R = 80$  nm in a cubic box of volume  $V$  with packing fraction  $\phi = 4\pi\rho R^3/3 = 0.01$  where  $\rho = N_p/V$  is the number density. We carry out MC simulation using local metropolis algorithm at  $T = 298$  K. Particles interact via a short-range potential defined by eq. (7). We study five different pairs of  $\zeta$ -potential and  $\sigma$  values, comparable to typical values measured in liposome solutions [12, 13]. We choose  $1/\kappa = 10$  nm. We recall that the value of the screening length does not modify the barrier height.

In our analysis, we invoked the capillarity approximation, in which each cluster is treated as a drop of uniform matter [24]. More precisely, when two approaching particles ( $A$  and  $B$ ) overcome the potential barrier (surface gap distance  $H < H_{\max}$ ), they aggregate forming a unique particle with radius  $R = (R_A^3 + R_B^3)^{1/3}$  and positioned in the center of mass of two aggregating spheres. We also assume that  $S$  (the size of the uniform potential regions

on the particle surface in the Velegol-Thwar expression) is independent of the cluster size.

To a first approximation, this approach can be justified by the fact that liposomes are relatively soft and the polyion-induced aggregation occurs forming structures of approximately spherical shape, as can be seen by means of transmission electron microscopy (TEM) measurements [2] and, even if in a more indirect way, confirmed by dynamic light scattering (DLS) measurements [25]. The compactness of the resulting aggregates suggests that, during the cluster formation, the entire new structure could interact with the approaching liposomes, acting as a unique spheroidal object with a mean effective curvature radius (oil-drop-like model). Under these assumptions, liposome aggregates contribute to the pair interaction potential with, on average, a surface charge distribution similar to the one of the single liposome.

To incorporate in the MC algorithm a Brownian dynamics, the  $i$ -th particle is selected with a probability proportional to  $R_0/R_i$ , where  $R_0$  is the initial radius and  $R_i$  is the radius of the  $i$ -th aggregate [26–28]. Each selected aggregate is moved in each direction by a random quantity uniformly distributed between  $\pm 0.2$  nm. Simulations have been carried out by varying both the  $\zeta$ -potential and the variance  $\sigma^2$ . The  $\zeta$ -potential values have been chosen similar to the typical ones measured in different colloidal systems (see fig. 1 and refs. [9, 10]). On the contrary, values for  $\sigma^2$ , in the absence of any experimental indication, have been chosen a little bit arbitrarily, but within the validity of the model and in any case within a range of reasonable values. The aggregation process progressively slows down and simulations are interrupted when a plateau in the time dependence of the aggregate average radius or mass is reached.

### 4 Results and discussion

In figs. 6 and 7, we present results of the aggregation process investigated for different values of the characteristic parameters ( $\zeta$ -potential and standard deviation  $\sigma$ ).

First, we will discuss the time evolution of the mean cluster radius at constant  $\sigma$  on varying the  $\zeta$ -potential. Figure 6 shows that on increasing the  $\zeta$ -potential, the aggregation process slows down and that the aggregates reach at long time a final limiting size. The slowing down of the dynamics is already seen at the early stage of the aggregation process, as shown in the inset of fig. 6, consistent with the effect of  $\zeta$ -potential on the height of the potential barrier.

Figure 7 shows the complementary case, *i.e.*, the effect of the different values of the standard deviation  $\sigma$  at a constant value of the  $\zeta$ -potential. Again, data confirm that the increase of the random fluctuations of the charges on the particle surface speeds up the aggregation process. In all the cases investigated, the growth process slows down at long times and aggregates appear to reach a long-time limit value, providing a strong evidence for a dynamics slow down and an arrest on the timescale sampled by our simulation. This finding suggests that, in this

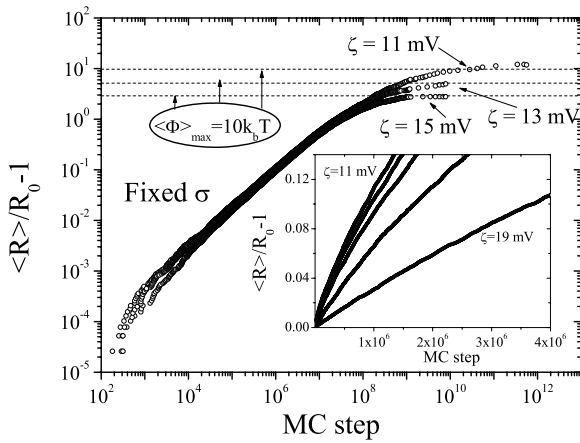


**Fig. 6.** Some typical time evolution of normalized mean cluster radius  $\langle R \rangle / R_0 - 1$ . Simulations have been carried out for different values of the  $\zeta$ -potential (in the range from 11 to 19 mV) with a constant value of the standard deviation  $\sigma = 15$  mV. The inset shows, in a linear scale, the evolution at short times of the mean size of the aggregates for different values of the  $\zeta$ -potential ( $\zeta = 11, 13, 15, 17, 19$  mV, from top to bottom, respectively).

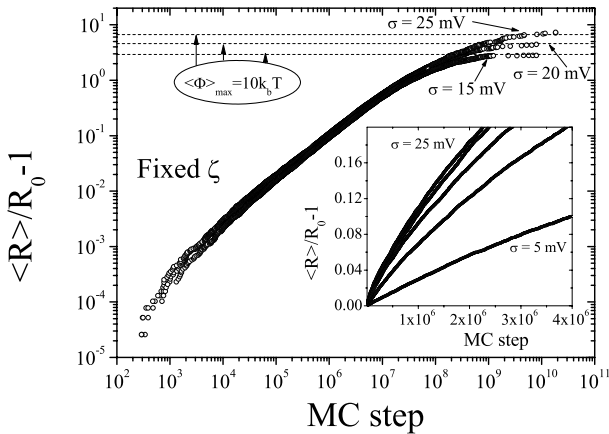


**Fig. 7.** Some typical time evolution of normalized mean cluster radius  $\langle R \rangle / R_0 - 1$ . Simulations have been carried out for different values of the standard deviation  $\sigma$  (in the range from 5 to 25 mV) with a constant value of the  $\zeta$ -potential  $\zeta = 15$  mV. The inset shows, in linear scale, the evolution at short times of the mean size of the aggregates, for different values of the standard deviation  $\sigma$  ( $\sigma = 25, 20, 15, 10, 5$  mV, from top to bottom, respectively).

class of systems, a kinetically arrested state can be generated by the coupling between the aggregates size and the electrostatic barrier. An estimate of the characteristic size reached by the aggregates at long time can be calculated assuming that the arrest is observed on the explored time scales when the interaction energy barrier reaches an *ad hoc* value. Indeed, inverting eq. (8), the relation connecting the radius of interacting aggregates and the potential barrier is easily obtained. We find that, in all the cases investigated, for all the couples of  $\zeta$ -potential and standard deviation  $\sigma$  values we have considered, the plateau

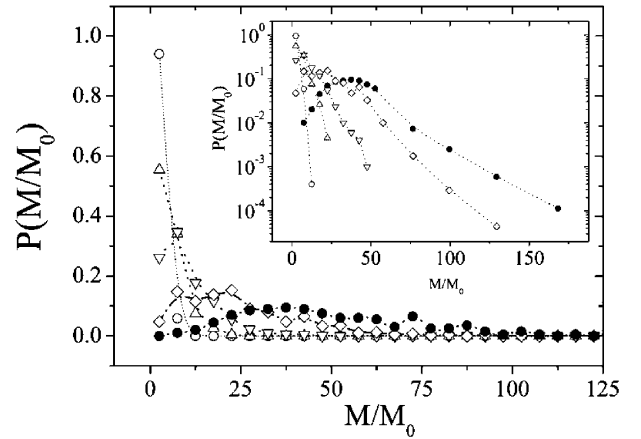


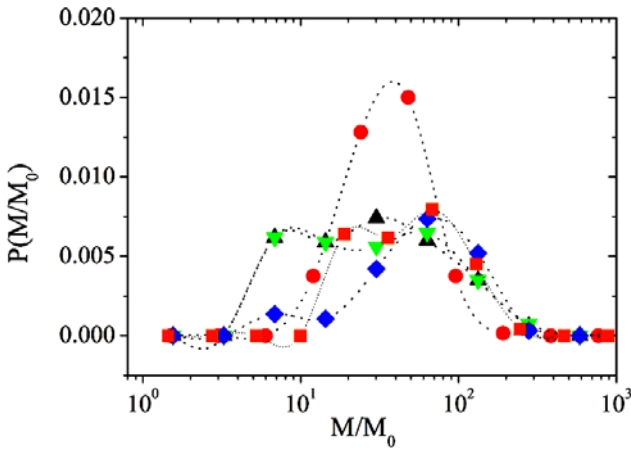
**Fig. 8.** Cluster size distribution of the mass  $M$  of the aggregating particles normalized to the mass  $M_0$  of the initial particles at different aggregation states for  $\zeta = 15$  mV and  $\sigma = 15$  mV.  $\circ$ :  $\langle M \rangle / M_0 = 2$ ;  $\triangle$ :  $\langle M \rangle / M_0 = 5$ ;  $\nabla$ :  $\langle M \rangle / M_0 = 10$ ;  $\diamond$ :  $\langle M \rangle / M_0 = 25$ ;  $\bullet$ :  $\langle M \rangle / M_0 = 50$ . Inset: the same distributions in a semi-log scale.

of the average aggregate size corresponds to a characteristic barrier  $\langle \Phi \rangle_{\max}$  of the order of about  $10 k_b T$  (see figs. 6 and 7, where the normalized size  $\langle R \rangle / R_0 - 1$  calculated from eq. (8) for different values of the  $\zeta$ -potential at fixed  $\sigma$  or conversely, for different values of  $\sigma$  at fixed  $\zeta$ -potential is shown).

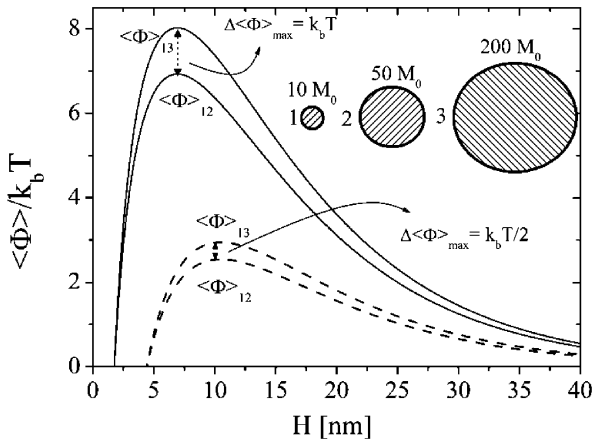
It is worth noting that both  $\zeta$  and  $\sigma$  values are assumed to be constant during the aggregation process. This assumption is justified as a consequence of the local character of the interaction, where only a local charge distribution determines the repulsive and attractive components of the pair potential. The distribution of the local charge of the elementary unit surfaces (single liposome) can be considered independent of the size of clusters.

Figure 8 shows the cluster mass distributions at different stages, during the aggregation process for the case of the couple of parameters  $\zeta = 15$  mV and  $\sigma = 15$  mV. The system evolves from the initial monodisperse distribution toward a broader distribution characterized by a well-defined peak, whose position increases with time. The distribution freezes when the system kinetically arrests. The inset in fig. 8 shows the same distribution in a semi-log scale to highlight the presence of a distribution tail compatible with an exponential distribution. Similar behavior is observed for all the cases investigated. The main differences concern the shape of the distributions in the arrested states, some of which are shown in fig. 9. The final size distribution has a smaller standard deviation  $\sigma_M$  in the case of higher values of the  $\zeta$ -potential or lower values of  $\sigma$ . The average mass instead shows an opposite trend, *i.e.*, it increases for smaller values of the  $\zeta$ -potential or higher values of  $\sigma$ .

A possible explanation of the influence of the electrostatic parameters,  $\zeta$ -potential and standard deviation  $\sigma$ , on the variance  $\sigma_M$  of the cluster size distribution is provided in fig. 10. Here, we compare the potential pro-



**Fig. 9.** (Color online) Cluster mass distribution in a log-scale for the cluster distributions closest to the arrested state;  $\bullet$ :  $\zeta = 15$  mV,  $\sigma = 15$  mV;  $\blacksquare$ :  $\zeta = 13$  mV,  $\sigma = 15$  mV;  $\blacktriangle$ :  $\zeta = 11$  mV,  $\sigma = 15$  mV;  $\blacklozenge$ :  $\zeta = 15$  mV,  $\sigma = 20$  mV;  $\blacktriangledown$ :  $\zeta = 15$  mV,  $\sigma = 25$  mV.



**Fig. 10.** The influence of the particle size on the interaction potential  $\langle\Phi\rangle$ . The graph shows the case of a particle “1” (with mass  $10M_0$ ) interacting with particle “2” (with mass  $50M_0$ ) and particle “3” (with mass  $200M_0$ ), respectively, for two different values of the  $\zeta$ -potential:  $\zeta = 11$  mV (dashed lines),  $\zeta = 15$  mV (full lines). As can be seen, particle “1” preferentially aggregates with particle “2” rather than with particle “3”, to which corresponds a higher potential barrier.

files (eq. (7)) when a particle interacts with particles of different sizes, for two different values of the  $\zeta$ -potential (11 and 15 mV, respectively). The results show that there is a preferential aggregation which favors the increase of smaller clusters rather than the increase of clusters of larger size. Indeed, the inter-particle potential (eq. (7)) predicts that the test particle (particle of mass  $10M_0$  in the example sketched in fig. 10) preferentially interact with clusters of smaller size (particle of mass  $50M_0$ ) rather than with clusters of larger size (particle of mass  $200M_0$ ). This kind of preferential interaction, which becomes relatively more and more favorable for larger values of the  $\zeta$ -potential, favors the aggregation of the smaller clusters

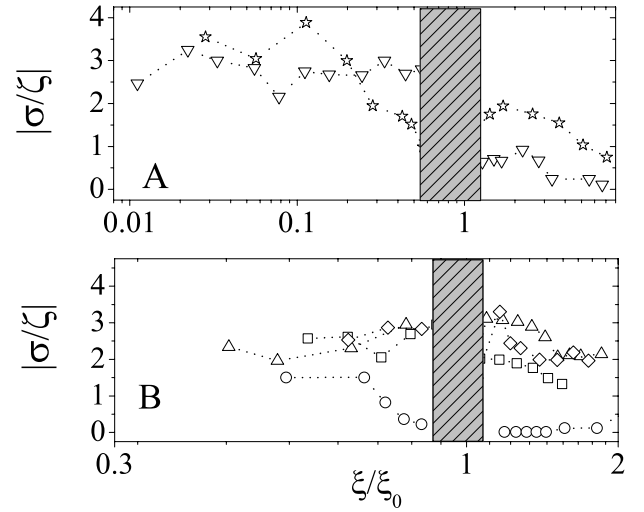


**Fig. 11.** The ratio  $|\sigma/\zeta|$  calculated from eq. (8) on the basis of the experimental values of radius  $R$  and the  $\zeta$ -potential of the aggregates formed in different polyion-induced particle aggregations in the case of soft particles. The marked regions correspond to the experimental instability of the aggregates, where their average size increases with time, until, in long time limit, they flocculate. A: Positive charged particles:  $\nabla$ : DOTAP liposomes (0.8 mg/ml) and polyacrylate sodium salt;  $\star$ : DOTAP liposomes (1.7 mg/ml) and polyacrylate sodium salt [12]. B: Negative charged particles:  $\circ$ : hybrid niosomes and  $\alpha$ -polylysine;  $\triangle$ : hybrid niosomes and  $\epsilon$ -polylysine;  $\diamond$ : hybrid niosomes and PEVP (ionization degree 95%) [13]. Hybrid niosomes are built up by Tween20, cholesterol and dicethylphosphate and the cationic polyion PEVP is Poly[*N*-ethyl-4-vinyl pyridinium] bromide.

in the system. These privileged interactions result in the formation of aggregate size distributions whose width decreases with increasing the  $\zeta$ -potential or with decreasing the  $\sigma$  values, as shown in fig. 9.

## 5 Comparison with experimental data

Equation (8) provides a connection between the experimentally measured values of the radius  $R$  (re-entrant condensation) and the  $\zeta$ -potential (charge inversion) of the cluster aggregates and the unknown value of the variance  $\sigma^2$  of the surface potential  $\psi$  (or, equivalently, the  $\zeta$ -potential). For example, the variance  $\sigma^2$  can be evaluated for the different systems shown in fig. 1 (cationic particles in the presence of anionic polyions and, conversely, anionic particles in the presence of cationic polyions). Figure 11 shows the dependence of the standard deviation  $\sigma$ , normalized to the value of the  $\zeta$ -potential,  $|\sigma/\zeta|$ , as a function of the normalized molar charge ratio  $\xi/\xi_0$ . Here,  $\xi$  is defined as the ratio between the polyion and lipid molar concentrations and  $\xi_0$  is the value of  $\xi$  at which the  $\zeta$ -potential goes to zero. As can be seen, there is a more or less pronounced decrease of  $|\sigma/\zeta|$  as a function of charge ratio  $\xi/\xi_0$  for all the systems investigated, as one can ex-

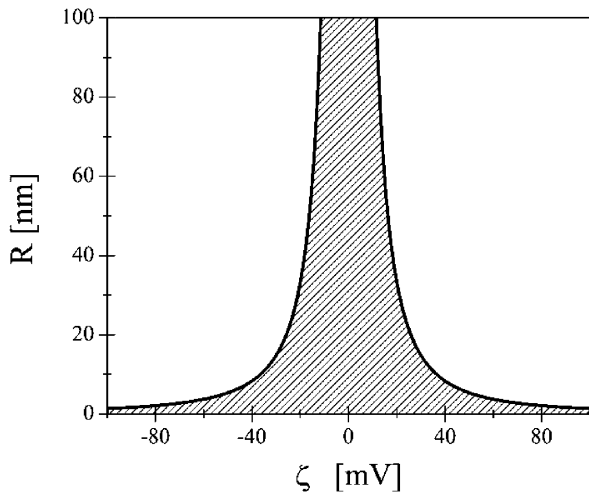


**Fig. 12.** Prohibited region under the curve defined by expression (11) for  $T = 298$  K and permittivity  $\epsilon$  of water.

pect when more and more polyion adsorption results in a more uniform charge distribution at the particle surface.

A final comment is in order. Experimentally, in some of the colloidal systems investigated, we have observed that, very close to the point of charge inversion ( $\xi/\xi_0 = 1$ ), the aggregates do not reach an equilibrium radius but, on the contrary, their size increases continuously with time until, in the long time limit, a complete flocculation occurs. In these conditions, huge aggregates form that ultimately flocculate. The range of the values of  $\xi/\xi_0$  where flocculation occurs is indicated in fig. 11 (shaded region). This instability corresponds to situations in which eq. (8), assuming, as previously done, a suitable value for the potential barrier height ( $\Phi_{AB} \simeq 10 k_b T$ ), cannot be satisfied for any plausible value of the parameter  $\sigma$ . The limiting size of the aggregates corresponding to  $\sigma \rightarrow 0$  results

$$R = \frac{10k_b T}{\pi \epsilon \zeta^2 \ln 4}. \quad (11)$$

This relationship marks off a region (instability region, shaded area in fig. 12) where the average size of the aggregates, for each possible value of the  $\zeta$ -potential, differs from the equilibrium value. In other words, in that region, real (physically meaning) values of  $\sigma$ , for which the size  $R$  (eq. (8)) is a kinetically stabilized radius, does not exist. This picture is strengthened by the experimental results of fig. 11 where the values of  $\sigma$  obtained from eq. (8) with the data of fig. 1 (the radius from the re-entrant condensation and  $\zeta$ -potential from the charge inversion) are shown. In the interval of  $\xi/\xi_0$  close to unity, with the values of the aggregate size measured just before the flocculation, no value of the parameter  $\sigma$  satisfies eq. (8). Forbidden values of  $\sigma$  close to the point of charge inversion ( $\xi/\xi_0 = 1$ ) point out that the measured size is too small to be considered as a kinetic equilibrium size. Notably, these values fall exactly in the instability region shown in fig. 12. Thus, the Velegol and Thwar potential provides support for the

evidence of an unstable region, in close agreement with the experimental results and allows us to evaluate if the measured size of the clusters can be considered or not a kinetically stabilized value. The fact that the presence of an instability region, effectively observed close to the isoelectric point, might be connected to the non-uniformity of the charge distribution on the particle surface, represents a helpful hint to address further studies on these colloidal systems.

## 6 Conclusions

A large body of experimental [1,2,12], theoretical [8–10] and simulation [29] investigations have shown that linear flexible or semiflexible polyions induce the aggregation of oppositely charged colloidal particles displaying a large variety of possible structures, thus emphasizing the many facets of charged macroion complex formation. Among these structures, clusters of liposomes stuck together by oppositely charged polyions form a class of model colloids in soft-matter physics which are of great importance in many biotechnological implications. In these cases, the attractive interaction contribution to the inter-particle potential is originated by a correlated adsorption at the particle surface, which causes a non-homogeneous charge distribution at the particle surface.

Since the major driving force of these processes is of electrostatic origin [30], more refined interaction potentials should be used to take into account some peculiar features in the aggregate cluster formation. We have modeled particle interactions by means of a mean-force inter-particle potential recently proposed by Velegol and Thwar, who developed a closed form analytical model to estimate the effect of a non-uniform charge distribution. Within the scenario of polyion-induced charged-particle aggregation, this potential provides a justification for why an attractive contribution arises in like-charged particle interactions in the presence of charge heterogeneities on the charged surface.

Monte Carlo simulations have been carried out for an ensemble of particles interacting via a Velegol and Thwar potential, for different values of the parameters characterizing the system. Simulations qualitatively reproduce all experimentally observable trends in a variety of different colloidal systems, from positively charged liposomes in the presence of anionic polyions to negatively charged hybrid niosomes in the presence of cationic polyions. This basic phenomenology is present both in *soft* aggregates, such as liposome clusters, and in *solid* particle aggregates, such as polystyrene sphere aggregates. In particular, simulations clearly evidence the formation of an arrested cluster phase, which is the sign of a kinetic arrested state in low-density colloidal suspensions.

For electrostatically highly coupled systems, the use of the Velegol and Thwar potential offers an interesting promise for the understanding of the role of electrostatic attractive and repulsive interactions between charged colloidal particles and oppositely charged polyions.

## References

1. F. Bordi, C. Cametti, S. Sennato, D. Viscomi, *J. Chem. Phys.* **126**, 024902 (2007).
2. F. Bordi, C. Cametti, M. Diociaiuti, S. Sennato, *Phys. Rev. E Rapid Commun.* **71**, 050401 (2005).
3. A. Yaroslavov, A. Rakhnyanskaya, Y. Ermakov, T. Burova, V.Y. Grinberg, F.M. Menger, *Langmuir* **23**, 7539 (2007).
4. D. Volodkin, V. Ball, P. Schaaf, J.C. Voegel, H. Möhwald, *Biochim. Biophys. Acta* **1768**, 280 (2007).
5. D. Napper, *Polymeric Stabilization of Colloidal Dispersion* (Academic, London, 1983).
6. J.H. Felgner, R. Kumar, C.N. Sridhar, C.J. Wheeler, Y.J. Tsai, R. Border, P. Ramsey, M. Martin, P.L. Felgner, *J. Biol. Chem.* **269**, 2550 (1994).
7. J. Felgner, *Proc. Natl. Acad. Sci. U.S.A.* **84**, 7413 (1987).
8. T.T. Nguyen, B.I. Shklovskii, *J. Chem. Phys.* **114**, 5905 (2001).
9. T. Nguyen, A. Grosberg, B. Shklovskii, *Phys. Rev. Lett.* **85**, 1568 (2000).
10. A.Y. Grosberg, T. Nguyen, B.I. Shklovskii, *Rev. Mod. Phys.* **74**, 329 (2002).
11. M.P.D. Lima, S. Simoes, P. Pires, H. Faneca, *Phys. Rev. E* **71**, 050401 (2005).
12. F. Bordi, C. Cametti, S. Sennato, D. Viscomi, *Phys. Rev. E Rapid Commun.* **74**, 030402R (2006).
13. S. Sennato, F. Bordi, C. Cametti, C. Marianecchi, M. Carafa, *J. Phys. Chem. B* **112**, 3702 (2008).
14. S. Zuzzi, C. Cametti, G. Onori, *Langmuir* **24**, 6024 (2008).
15. D. Truzzolillo, C. Cametti, S. Zuzzi, S. Sennato, in preparation (2008).
16. C.R. Safinya, K. Ewert, A. Ahmad, H.M. Evans, U. Raviv, D.J. Needleman, A.J. Lin, N.L. Slack, C. George, C.E. Samuel, *Philos. Trans. R. Soc. London, Ser. A* **364**, 2573 (2006).
17. C.R. Safinya, I. Koltover, J. Raedler, *Curr. Opin. Colloid Interface Sci.* **3**, 69 (1998).
18. S. Sennato, F. Bordi, C. Cametti, M. Diociaiuti, P. Malaspina, *Biochem. Biophys. Acta.* **1714**, 11 (2005).
19. E.J.W. Verwey, J.T.G. Overbeek, *Theory of the Stability of Lyophobic Colloids* (Elsevier, Amsterdam, 1948).
20. J. Mou, D. Czajkowsky, Y. Zhang, Z. Shao, *FEBS Lett.* **371**, 279 (1995).
21. D. Velegol, P.K. Thwar, *Langmuir* **17**, 7687 (2001).
22. R. Hogg, T.W. Healy, D.W. Fuerstenau, *Trans. Faraday Soc.* **62**, 1638 (1966).
23. R. Tadmor, *J. Phys.: Condens. Matter* **13**, L195 (2001).
24. A.M. Puertas, G. Odriozola, *J. Phys. Chem. B* **111**, 5564 (2007).
25. J. Sabin, G. Prieto, J. Ruso, P. Messina, F. Sarmiento, *Phys. Rev. E* **76**, 011408 (2007).
26. S. Babu, M. Rottureau, T. Nicolai, J.C. Gimel, D. Durand, *Eur. Phys. J. E* **19**, 203 (2006).
27. S. Babu, M. Rottureau, J.C. Gimel, T. Nicolai, *J. Chem. Phys.* **125**, 184512 (2006).
28. B.H. Zimm, *J. Chem. Phys.* **24**, 269 (1956).
29. R. Messina, C. Holm, K. Kremer, *Phys. Rev. E* **65**, 041805 (2002).
30. G. Gillies, W. Lin, M. Borkovec, *J. Phys. Chem. B* **111**, 8626 (2007).